

# Improved simulations of the planetary nebula luminosity function

R.H. Méndez and T. Soffner

Institut für Astronomie und Astrophysik der Universität München, Scheinerstr. 1, D-81679 Munich, Germany

Accepted November 1996

arXiv:astro-ph/9611128v1 17 Nov 1996

**Abstract.** We have developed a new procedure for the generation of a planetary nebula luminosity function (PNLF), improving on previous work (Méndez et al. 1993). The procedure is based, as before, on an exponential central star mass distribution, on H-burning post-AGB evolutionary tracks, and on the *avoidance* of nebular models for the calculation of nebular fluxes. We have added new post-AGB evolutionary tracks and introduced the following improvements: (1) the imperfect analytical representation of post-AGB evolutionary tracks has been replaced by an interpolation routine giving a better approximation; (2) we have modified the distribution of the intensities of [O III]  $\lambda 5007$  relative to  $H\beta$ , so that it better imitates the observed distribution, which we have taken from data in the Strasbourg-ESO catalogue of Galactic PNs and other sources; (3) we have adjusted the absorbing factor  $\mu$  along the white dwarf cooling tracks, so as to reproduce the observed PNLF of the Magellanic Clouds and M 31 at fainter magnitudes. In this way we have produced a PNLF which is more consistent with observed PN properties. We use this randomly generated PNLF to: (1) show as convincingly as possible that most PNs in any real population must leak stellar H-ionizing photons; (2) revise our determinations of the parameter  $\mu_{\max}$ ; (3) discuss the shape of the PNLF, hinting at the possible existence of a distinct feature 2 magnitudes fainter than the brightest PNs; (4) attempt estimates of maximum final masses from fits to the PNLFs of the LMC and M 31. There is marginal evidence of a higher maximum final mass in the LMC, but this should be confirmed in other galaxies with recent star formation. A convincing confirmation will require to increase the sample sizes and to extend the PNLFs to at least 1.5 mag fainter than the brightest PNs.

**Key words:** planetary nebulae: general, luminosity function – stars: post-AGB – galaxies: distances – methods: numerical

## 1. Introduction

In a previous paper (Méndez et al. 1993, in what follows MKCJ93) a procedure was described for the numerical simulation of the bright end of the planetary nebula luminosity function (PNLF). The purpose was to model the PNLF in such a way as to make it possible to study the effects, on the

observed bright end of the PNLF, of the following: (1) sample size; (2) time elapsed since last episode of substantial star formation; and (3) incomplete nebular absorption of stellar H-ionizing photons. This motivation (in particular the desire to study optical thickness effects) led to the choice of a method characterized by the avoidance of nebular models for flux calculations. In fact, the spectacular images of several nearby PNs, produced by the Hubble Space Telescope, have recently added to the current uncertainties concerning the transition time between the AGB and the moment when the central star becomes hot enough to ionize the nebula in supporting our feeling that current nebular modeling cannot accurately predict how able is the nebula to absorb all the H-ionizing photons from the central star, and how will this ability evolve with time. This explains our selection of an approach based, as much as possible, on *observed* properties of PNs and their central stars.

In the present paper we introduce several improvements in the PNLF simulations, in preparation for the moment when better and deeper PNLFs will be obtainable with the new 8m-class telescopes now in construction. The purpose of these improved PNLF simulations is to further develop the PNLF as a tool, not only for the accurate measurement of extragalactic distances, but also for studies of the initial-to-final mass relation and related mass loss processes in luminous galaxies with and without recent star formation. There has been abundant research on the reliability of the bright end of the PNLF as a secondary distance indicator (see e.g. Jacoby 1997), showing that there is excellent agreement between cepheid and PNLF distances. This might be interpreted as an indication that the bright end of the PNLF is not significantly affected by population characteristics. However, it is also possible (and perhaps more plausible) to argue (e.g. Feldmeier et al. 1997) that most PN searches in galaxies with recent star formation have been made in such a way as to avoid severe contamination with H II regions, discriminating in this way against the inclusion of the potentially most massive central stars, which would tend to be closer to such regions. The best way of resolving this ambiguity is through PN searches that do not discriminate against H II regions, like those in NGC 300 (Soffner et al. 1996). We believe that a reduction of the statistical noise through increased sample sizes, as well as an extension of the PNLF towards fainter magnitudes, should render population effects detectable through differences in the shape of the PNLF, as described in MKCJ93. Better simulations will allow us to predict more confidently what population effects should be detectable in practice. In parallel, the constraints derived from comparisons of

*Send offprint requests to:* R.H. Méndez

simulated with observed PNLFs will test how successful we are in modeling the PNLF using an approach partly based on random numbers, and will allow us to further refine the PNLF simulations. In the end, even if population effects are not detectable, we may be able to understand why.

Sections 2 to 5 describe the improvements we have introduced in our simulations, and in Sect. 5 we show that most PNs in any real population must leak stellar H-ionizing photons. Sect. 6 describes a few consistency checks that have been made or can be made in principle. In Sect. 7 we discuss the shape of the PNLF, and in Sect. 8 we describe an attempt to determine maximum post-AGB final masses in the Large Magellanic Cloud (LMC) and in the bulge of M 31.

## 2. The improvements

The basic idea of the procedure for the PNLF simulation is the same as in MKCJ93, to which we refer the reader for details. We generate a set of PNs with random post-AGB ages and central star masses. The ages are given by a uniform random distribution from 0 to 30 000 years, counting from the moment when the central star has  $T_{\text{eff}} = 25\,000$  K. The central star masses are given by an exponential random distribution selected to reproduce the observed white dwarf mass distribution in our Galaxy (see Fig. 4 in MKCJ93). More recent research keeps showing an exponential tail in the white dwarf mass distribution (see e.g. Bragaglia et al. 1995), and therefore we are confident that this feature remains valid in cases with more or less constant star formation. As we will explain later, cases without recent star formation are simulated by truncating the mass distribution at a certain maximum final mass. For each PN in the set we have, then, a pair of random numbers giving mass and age of the central star. These random numbers are input to a routine that gives the corresponding luminosity  $L$  and  $T_{\text{eff}}$  of the central star. Our first improvement is to replace the analytical representation of post-AGB tracks used in MKCJ93 by an interpolating routine that gives a better approximation. Knowing  $L$  and  $T_{\text{eff}}$  we calculate, using recombination theory, the  $H\beta$  luminosity that the nebula would emit if it were completely optically thick in the H Lyman continuum. Then we generate a random number, subject to several conditions (derived from observations of PNs and their central stars, see MKCJ93), for the absorbing factor  $\mu$ , which gives the fraction of stellar ionizing luminosity absorbed by the nebula. Using the absorbing factor we correct the  $H\beta$  luminosity. Our second improvement concerns the generation of suitable absorbing factors for PNs on cooling tracks. Finally, we produce  $[O\text{ III}]\lambda 5007$  fluxes from the previously derived  $H\beta$  fluxes. This is done by generating another random number, again subject to several conditions, for the intensity of  $\lambda 5007$  relative to  $H\beta$ . The introduction of more stringent conditions for this intensity ratio, derived from a larger database, is our third improvement. In what follows we describe all these changes in more detail. We believe that the description will be more easily followed if we discuss the  $\lambda 5007$  intensities before dealing with the absorbing factor  $\mu$ . Stellar masses and luminosities are expressed in solar units.

## 3. Improved representation of post-AGB tracks

As in MKCJ93, we base our simulations on the H-burning post-AGB tracks of Schönberner (1989) and Blöcker & Schönberner (1990). We have added new H-burning tracks recently published by Blöcker (1995). Since we were not satisfied with the

analytical representation used in MKCJ93, especially concerning ages and luminosities on the white dwarf cooling tracks, we decided to implement some interpolation procedures. In addition to the tracks already mentioned, in order to guide the extrapolation for masses above 0.94 solar masses, we used an additional track for 1.2 solar masses, obtained by slightly modifying the ages in Paczynski's (1971) track so as to make them more consistent with the deceleration of the evolution that takes place along the Blöcker & Schönberner 0.836 solar mass cooling track.

We used the available evolutionary tracks to construct a look-up table giving  $\log T_{\text{eff}}$  and  $\log L$  for 3000 ages between 0 and 30 000 years and for 260 masses between 0.55 and 1.2 solar masses. Let us explain the construction of this look-up table; we used different methods for the required calculations in different regions of the  $\log L - \log T_{\text{eff}}$  diagram.

For temperatures between 25 000 and 72 000 K, where the tracks run almost horizontally, we plotted (1)  $\log(\text{age})$  and (2)  $\log L$  as functions of mass for a given  $T_{\text{eff}}$ , using information derived from the known tracks; fitted  $\log(\text{age})$  and  $\log L$  curves as functions of mass; and derived age and  $L$  for the 260 masses. The procedure was repeated for 40 temperatures in this region.

For luminosities below  $\log L = 3.0$ , which is the region of the white dwarf cooling tracks, we plotted (1)  $\log(\text{age})$  and (2)  $\log T_{\text{eff}}$  as functions of mass for a given  $L$ ; fitted  $\log(\text{age})$  and  $\log T_{\text{eff}}$  curves; and derived age and  $T_{\text{eff}}$  for the 260 masses. The procedure was repeated for 30 luminosities in this region.

For the remaining region (the knees of the tracks) we produced fits along 40 straight lines radiating from a point with  $\log T_{\text{eff}} = 4.86$  and  $\log L = 3.0$ . These lines cross the tracks at approximately right angles. In this case it was of course necessary to plot  $\log(\text{age})$ ,  $\log L$  and  $\log T_{\text{eff}}$  as functions of mass, and fit curves for the 3 parameters. From these curves we obtained age,  $L$  and  $T_{\text{eff}}$  for the 260 masses, along each of the 40 lines we had defined.

Finally, the full look-up table ( $\log T_{\text{eff}}$  and  $\log L$  for 260 masses and 3000 ages) was completed for the missing ages using interpolation along each track.

The look-up table was used in the following way: after generating the two random numbers giving mass and age, the four neighboring values of age and mass in the table were identified, and the values for  $\log T_{\text{eff}}$  and  $\log L$  were derived using bilinear interpolation. Fig. 1 shows examples of evolutionary tracks generated for several masses, and Fig. 2 shows the positions of 1500 randomly generated central stars in the  $\log L - \log T_{\text{eff}}$  diagram. These two figures can be compared with Figs. 5 and 6 of MKCJ93.

In addition to a better representation of the post-AGB evolutionary tracks, the new procedure has the advantage that it is not tied to a specific set of post-AGB models; it can be applied (i.e. a new look-up table can be easily generated) for any preferred set of tracks.

We considered, but finally decided against, the inclusion of He-burning post-AGB tracks for our simulations. It would be good to allow for a certain percentage of such tracks, because the evolution is slower than for a H-burning star of the same mass. The basic problem is that the He-burning tracks are affected by loops and jumps produced respectively by the late thermal pulse and by the reignition of the H-shell (see e.g. Vassiliadis & Wood 1994, or Blöcker 1995). It would be necessary to make an enormous amount of evolutionary calculations in order to accurately reproduce the complexities of this behavior,

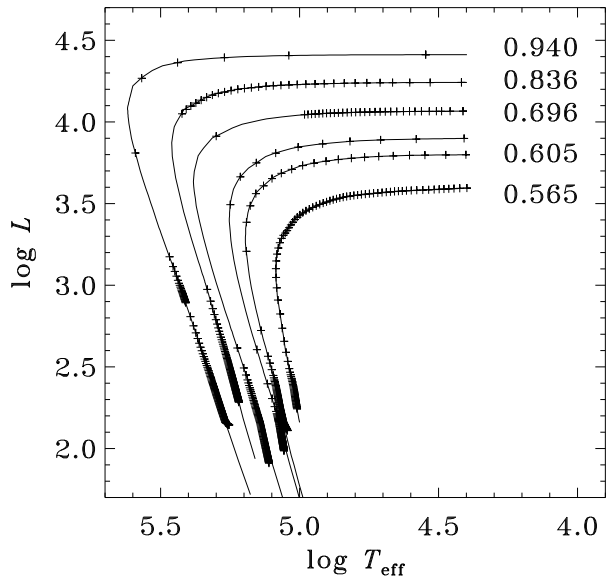


**Fig. 1.** The solid lines are post-AGB evolutionary tracks (H-burning) for 6 different central star masses, taken from Schönberner (1989) and Blöcker (1995). The unlabeled track is for 0.625 solar masses. We used also the track for 0.644 solar masses, but did not plot it to avoid overcrowding. The plus signs indicate central star luminosities and temperatures calculated, from our look-up table, for the same 6 masses at 100 post-AGB ages between 1 and 30 000 years (300-yr intervals). All ages are counted from the moment when the central star has a temperature of 25 000 K. For the 3 upper tracks we have added 30 ages between 1 and 300 yr (10-yr intervals) to obtain a better coverage of the fast evolution towards higher temperatures.

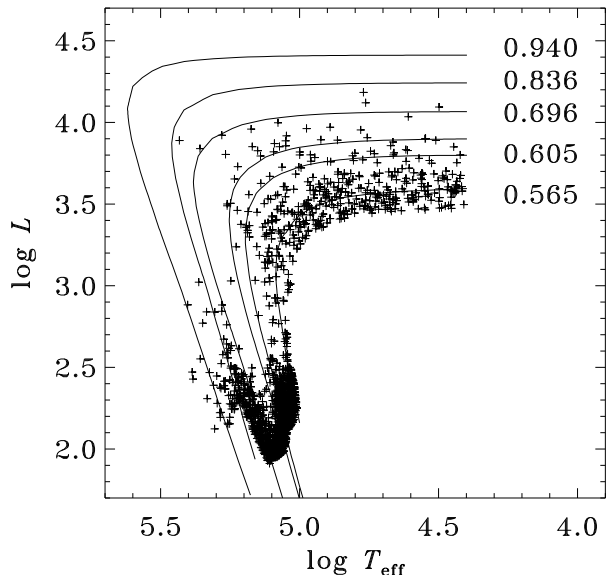


**Fig. 2.** The resulting values of luminosity and temperature for the central stars of 1500 randomly generated PNs, using the same exponential mass distribution as in MKCJ93.

which is dependent on the phase, in the thermal pulse cycle, at which the star leaves the AGB. No interpolation procedure appears to be viable in this case.

The situation would be probably simpler in the particular case of H-deficient central stars, which represent about 30% of the well-observed central stars in our Galaxy (see e.g. Méndez 1991). Obviously such stars must be He-burners, but in this case no H-shell reignition is expected, because no H is left, and the tracks may be more easily simulated. The problem is that the evolutionary status of these objects is not yet fully understood, and no reliable tracks are available.

In summary, given the present knowledge we are not likely to gain much from any attempt to include He-burners in our simulations, but we remark that this is a potential source of uncertainty in PNLF modeling.

#### 4. The observed distribution of $\lambda 5007$ relative intensities

One weak point in MKCJ93 was the rather schematic representation of the distribution of intensities of  $\lambda 5007$  relative to  $H\beta$ . We have generated a new distribution, by comparison with two observed distributions: one for 118 PNs in the LMC (data taken from Wood et al. 1987; Meatheringham et al. 1988; Jacoby et al. 1990; Meatheringham and Dopita 1991a, 1991b; Vassiliadis et al. 1992) and another one for 983 PNs in our Galaxy, taken from the Strasbourg-ESO Catalogue of Galactic PNs (Acker et al. 1992). In about 80 cases, where the Catalogue's  $\lambda 5007$  intensity was not given or unreliable, we have taken it from other sources, listed in the Catalogue.

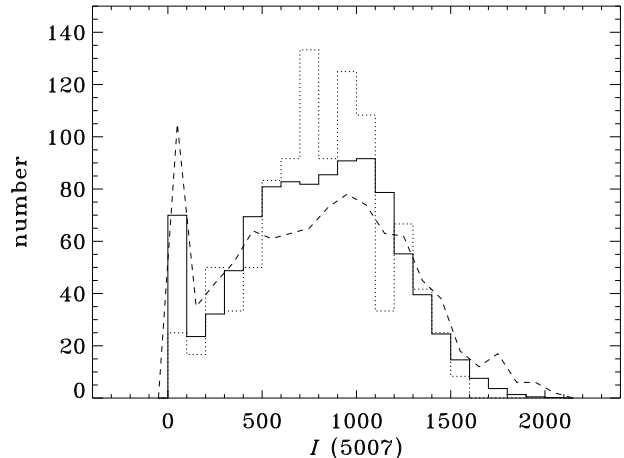


**Fig. 3.** Histograms of the intensity of  $\lambda 5007$  relative to  $H\beta$ , on the scale  $I(H\beta) = 100$ . The dashed line indicates the histogram for 983 objects in our Galaxy. The other two histograms have been normalized to this number. The dotted line is the histogram for 118 LMC objects. The full line is our simulated distribution, generated as described in the text.

Fig. 3 shows the observed distributions compared with our simulated distribution, which is produced by first generating a Gaussian centered at an intensity of 1000 (on the usual scale of  $I(H\beta) = 100$ ) with  $\text{FWHM}=300$ . Then, following the discus-

sion in Section 4 of MKCJ93 about low  $\lambda 5007$  values (see also Stasinska 1989), we decrease the  $\lambda 5007$  intensity to 50% of its randomly generated value for central stars on heating tracks which have masses smaller than 0.57 solar masses and  $T_{\text{eff}} > 75\,000$  K. In addition, for central stars with temperatures below 60 000 K we do not use the generated random number, but use instead Eq. (5) in MKCJ93. In this way we minimize the risk of randomly creating a PN with a  $\lambda 5007$  intensity which is incompatible with the properties of its central star.

Finally, we must compensate for an obvious selection effect: the observed distributions in our Galaxy and in the LMC are not likely to include PNs with very low- $L$  central stars, all of which have high temperatures; therefore, before plotting our simulated distribution we eliminate all PNs with central stars fainter than  $\log L = 2.4$  (see Fig. 2).

We would like to emphasize that the evolutionary tracks do not produce enough low- $T_{\text{eff}}$  central stars to explain the observed number of PNs with low  $\lambda 5007$  intensities. In order to illustrate this point, we can use our simulations. Let us adopt a limit of 500 for the intensity of  $\lambda 5007$ . According to Eq. (5) in MKCJ93, this limit corresponds to a stellar  $T_{\text{eff}} = 43\,000$  K. If we restrict again our attention to PNs with central stars brighter than  $\log L = 2.4$ , our simulations produce 15% of these central stars with  $T_{\text{eff}}$  below the limit, while 25% of the PNs have  $\lambda 5007$  fainter than 500. This means that about 40% of the PNs with faint  $\lambda 5007$  should have hot central stars.

Since there is insufficient direct information about  $T_{\text{eff}}$ , we have tried to test this prediction using the Strasbourg-ESO Catalogue and a recent catalogue of  $\lambda 4686$  line intensities (Tylanda et al. 1994). We have found that, of 275 PNs in the Strasbourg-ESO Catalogue with an intensity of  $\lambda 5007$  below 500, at least 20% show the He II  $\lambda 4686$  nebular emission, which indicates a stellar temperature above 45 000 K. This percentage is less than the 40% predicted, but on the other hand it is probably a lower limit, because in some cases a weak  $\lambda 4686$  line may be present but not detected in the surveys (in the catalogue of Tylanda et al. we find, among the 275 PNs with weak  $\lambda 5007$ , a further 25% for which the upper limit of the  $\lambda 4686$  intensity is 5 or higher, on the scale  $H\beta = 100$ ). Therefore, although the test cannot be considered to be sufficient for any definitive conclusion, given all the uncertainties involved, we think it indicates that our simulations have produced a useful first approximation to the observed variety of PN spectra.

As shown in Fig. 3, we now reproduce the observed distributions quite well. Notice in particular the Gaussian tail towards high intensities, which was not correctly reproduced in MKCJ93 (those simulations produced an excess of PNs below 1500, and no PN above 1500).

### 5. The absorbing factor $\mu$ : reproducing the observed PNLF to fainter magnitudes

Assume for a moment that all the PNs are completely optically thick. We can make a simulation based on this assumption, and compare the resulting PNLF with the observed PNLF of the LMC: see Fig. 4. The failure of the completely optically thick assumption is quite evident. The simulated PNLF, calculated for a sample size of 1000 objects (which is Jacoby's (1980) estimate for the total number of PNs in the LMC), reaches much brighter magnitudes. In order to force agreement by a horizontal shift of the observed PNLF, until it fits the simulated PNLF bright end, it would be necessary to adopt an implausible distance of 66 kpc for the LMC. An attempt to fit the

observed LMC PNLF at the right distance, by *vertically* shifting the simulated PNLF, would lead to a sample size of about 300, implausibly close to the total number of known PNs in the LMC. This makes it clear that the existence of many optically thin PNs at the bright end of the PNLF is an essential feature in our simulations. The introduction of the absorbing factor  $\mu$  in MKCJ93, using information independently derived from model atmosphere studies of central stars of PNs in our Galaxy (Méndez et al. 1992), immediately led to satisfactory fits of the PNLFs of the LMC and M 31. We have not modified the procedure described in MKCJ93 for the generation of  $\mu$  for PNs with high-luminosity central stars (namely, those on heating tracks). Here we just remind the reader that many, but not all, of the PNs with cooler central stars are allowed to have  $\mu=1$ , and that the procedure defines, for central stars on heating tracks and with temperatures above 40 000 K, a random distribution of  $\mu$  from 0.05 up to a parameter  $\mu_{\text{max}}$ . If  $\mu_{\text{max}}=1$ , then a small percentage of the bright PNs with hotter central stars can have  $\mu$  close to 1.

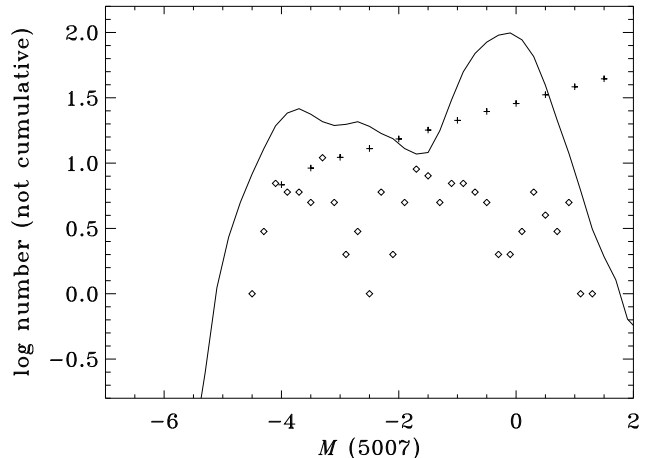


**Fig. 4.** A PNLF simulation for the LMC, assuming that all PNs are completely optically thick (for all objects  $\mu=1$ ). The diamonds represent the observed  $\lambda 5007$  PNLF of the LMC, from data collected in the literature (see text, Sect. 4). The LMC is assumed to be at a distance of 50 Mpc, and we adopt an average logarithmic extinction at  $H\beta$ ,  $c=0.19$  (Soffner et al. 1996). The magnitudes fainter than  $-3$  are obviously affected by severe incompleteness. We have adopted the extension towards fainter magnitudes (plus signs) from Fig. 1 of Ciardullo (1995). The solid line is the simulated PNLF, with data binned, like the observed ones, into 0.2 mag intervals. The sample size is 1000, and the maximum final mass is 0.7 solar masses (the exponential central star mass distribution is truncated at this mass). The choice of this maximum final mass will be explained in Sect. 8. Even with this truncation, the simulated PNLF has too many bright PNs and too few of the very faint ones. The discrepancy is solved by forcing many PNs to have small  $\mu$  values, as shown in Fig. 5.

Now we want to extend the simulated PNLF towards fainter magnitudes. This requires some additional information about  $\mu$  for PNs with central stars on cooling tracks. It is clear from Fig. 4 that not all PNs on cooling tracks can have  $\mu = 1$ , because that assumption produces an enormous hump in the PNLF at  $M(5007) \sim 0$ , and consequently also a pronounced

deficit of very faint PNs. The required information about  $\mu$  cannot be easily obtained from central star studies, because in this region of the HR diagram the central stars are intrinsically faint. We have therefore decided to adopt a simple procedure for the random generation of values of  $\mu$  at low central star luminosities, and adjust it by requiring agreement of the simulated PNLf at fainter magnitudes with the statistically complete PNLf inferred from PN observations in nearby galaxies (see e.g. Fig. 1 in Ciardullo 1995).

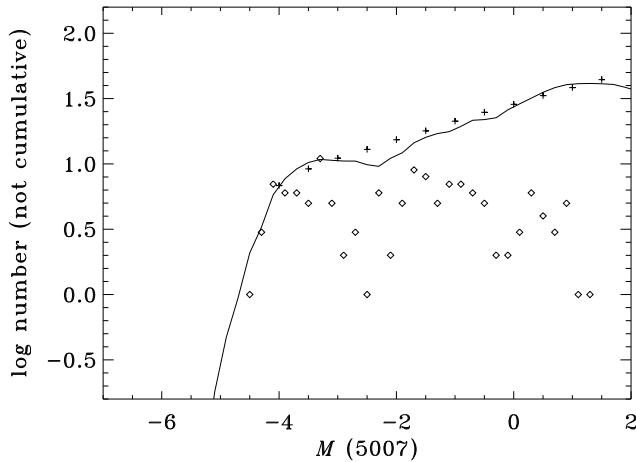


**Fig. 5.** Final simulation of the LMC PNLf. The same observed LMC PNLf used in Fig. 4 is now compared with our final simulation, which includes many PNs with small  $\mu$  values. Most of the PNs with high values of  $\mu$  have low-temperature central stars. We have adopted  $\mu_{\max} = 1$  (which allows some PNs on heating tracks and with temperatures above 40 000 K to be almost completely optically thick), sample size = 1000, and maximum final mass 0.7 solar masses.

The procedure we have implemented is quite simple. We estimate for each mass how much time it takes for the central star to reach the turnover point of its evolutionary track, that is to say the beginning of the cooling track. For all ages larger than this time, the absorbing factor  $\mu$  is set equal to a random number uniformly distributed between 0.1 and 1, and this number is multiplied by a factor  $(1 - (\text{age}/30\,000))$ . In this way we ensure that all absorbing factors tend to 0 as the nebula dissipates. Somewhat surprisingly, this simple procedure works very well. Fig. 5 compares the “observed” LMC PNLf with our final simulation, where we have set  $\mu_{\max} = 1$  for PNs with hot central stars on heating tracks. The sample size is 1000, in agreement with Jacoby’s (1980) estimate, and we have selected a maximum final mass equal to 0.7 solar masses (see MKCJ93). This choice of maximum final mass will be explained in Sect. 8.

It is interesting to note that the factor  $(1 - (\text{age}/30\,000))$  is necessary to achieve a reasonable representation of the PNLf. If we suppress this factor, then our simulations give a result very similar to that shown in Fig. 4.

The new value of  $\mu_{\max}$  for the LMC is higher than determined in MKCJ93 (0.6). There are two reasons for this change: the new distribution of  $\lambda 5007$  intensities, and the adoption of a higher reddening for the LMC, discussed by Soffner et al.

(1996). In next Section we subject our new simulation to a few consistency checks.

## 6. Consistency checks

In Fig. 6 we have plotted the  $H\beta$  LMC PNLf. In the same way as with the  $\lambda 5007$  PNLf, the simulation provides a good fit at the bright end, and severe incompleteness begins about one magnitude fainter. This indicates that the simulation is producing suitable values of the  $\lambda 5007 / H\beta$  ratio at the bright end of the PNLf. We can directly check this by extracting from the master simulation (208 000 objects) a random subsample of 1000 objects. In this subsample the average  $I(5007)$  for the 15 brightest PNs is 1181, in good agreement with the average intensity of 1213 for the 15 brightest observed PNs in the LMC. It is also interesting to know the values of  $\mu$  for the 15 brightest PNs in the simulated subsample: they are between 0.38 and 0.94, with an average 0.74. Thus we see that, although  $\mu_{\max}=1$ , the bright end of the PNLf is *not* dominated by PNs with  $\mu$  values very close to 1.

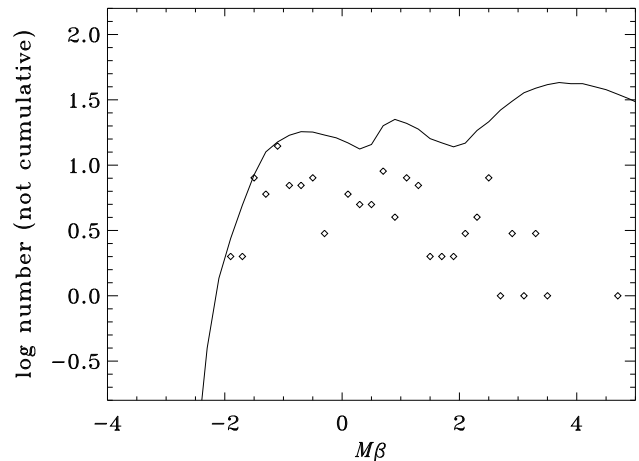


**Fig. 6.** The observed  $H\beta$  LMC PNLf, compared with a PNLf built from the same simulation used in Fig. 5:  $\mu_{\max} = 1$ , sample size = 1000, and maximum final mass 0.7 solar masses. There is a good fit to the bright end of the  $H\beta$  PNLf, although here a somewhat smaller sample size (800) would give a better fit. We find severe incompleteness in the observed PNLf for magnitudes fainter than  $-1$ . Thus the situation is very similar to that of Fig. 5.

This result leads us to rediscuss the interpretation of the observed presence of low-excitation PNs among those with the brightest values of  $M_\beta$  in the LMC (Figure 4a of Dopita et al. 1992). MKCJ93 concluded that this behavior had to be explained by a low value of  $\mu_{\max}=0.6$ . But now we see that this behavior can be produced by chance in cases where  $\mu_{\max}$  is higher. We have run more than 100 simulations for a sample size of 1000 objects and  $\mu_{\max}=1$ , and we find that in 30% of these simulations there are 2 PNs with  $I(5007) < 500$  among those PNs with the 9 brightest values of  $M_\beta$  (these numbers, 2 among 9, are what we find in our LMC database). For comparison, we have also run more than 100 simulations for 1000 objects with *all* values of  $\mu = 1$ , and in this case less than

7% of all simulations show 2 low-excitation PNs among the 9 brightest in  $H\beta$ .

In this way we see that any argument based on plots of  $I(5007)$  as function of  $M_\beta$  makes sense only if applied to a sufficiently large sample of galaxies. For example, if we were to find that of 10 galaxies the *majority* show low-excitation PNs among the brightest in  $H\beta$ , then we would be induced to believe that something must be inconsistent in our simulations. This is a test that may become possible in the near future. For the moment we consider that all the available information is consistent with the following general rule: many optically thin PNs, but  $\mu_{\max}=1$ , as implemented in our simulations.

One could argue that the use of  $I(5007)$ - $M_\beta$  plots to decide about  $\mu_{\max}$  would be further compromised by the possible existence of low-excitation PNs with hot central stars, as described in Sect. 4 above. Although this is true, we should point out that such objects are generally expected to have very low values of  $\mu$ , and are therefore unlikely to be among the brightest PNs in  $H\beta$ . For example, in the case of the LMC we have verified that the brightest low-excitation objects (SMP3, SMP5) do not show  $\text{He II } \lambda 4686$  nebular emission. This implies that the central star temperatures are indeed low.

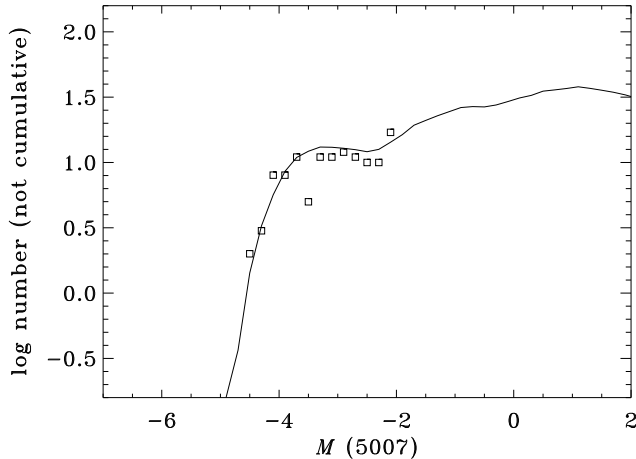


**Fig. 7.** The statistically complete  $\lambda 5007$  PNLF in M 31 (samples A + B of Ciardullo et al. 1989), adopting a distance of 770 kpc, compared with a simulated PNLF with  $\mu_{\max} = 1$ , sample size = 1000, and maximum final mass 0.63 solar masses. The choice of maximum final mass will be explained in Sect. 8. The change of slope at absolute  $\lambda 5007$  magnitude  $-2.3$ , predicted by our simulations, would seem to be reproduced by the data.

## 7. On the shape of the PNLF

Let us compare our simulated PNLF with the formula used by Ciardullo et al. (1989, see their Eq. (2)); their formula behaves like the plus signs in our Figs. 4 and 5). There is an interesting difference: while the formula of Ciardullo et al. gives an ever increasing PNLF towards fainter magnitudes, our simulation shows a roughly constant, or even decreasing, PNLF between  $M(5007) = -3.5$  and  $-2.3$ , and only starts increasing again for mags fainter than  $-2.3$ . This change of slope can be considered

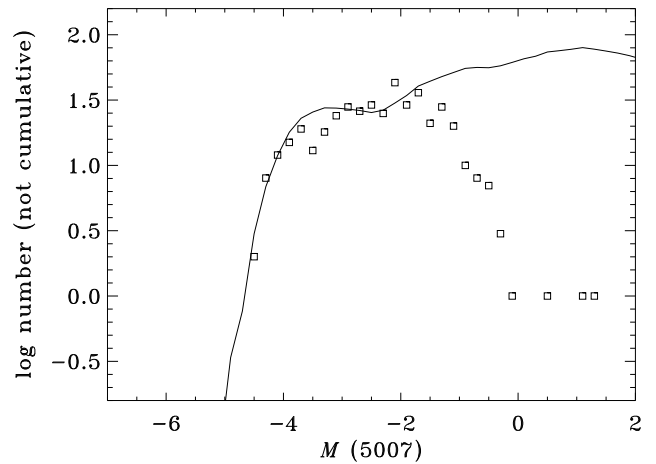


**Fig. 8.** The  $\lambda 5007$  PNLF of M 31 (all the 429 PNs measured by Ciardullo et al. 1989), compared with a simulated PNLF with  $\mu_{\max} = 1$ , sample size = 2100, and maximum final mass 0.63 solar masses. There is significant incompleteness at mags fainter than  $-1.5$ . Notice again the possible change of slope at  $-2.3$ .

a “prediction” of our simulation procedure. The LMC data are not suitable to test this prediction, because of the severe incompleteness at the relevant values of  $M(5007)$ . But the M 31 sample remains statistically complete until  $M(5007) = -1.5$ , and indeed Figs. 7 and 8 would seem to give a hint of support to our simulation (see also the combined PNLF shown by Jacoby 1997). However, the evidence is insufficient. It would be important to verify if the slope change at  $-2.3$  is present in other galaxies (this verification will become possible with 8-m telescopes) because (1) it would allow to test how reliable is our PNLF generation, eventually indicating if further adjustments are needed; (2) it would give more confidence about how to use the shape of the PNLF for distance determinations and for the study of population characteristics (to be discussed in next section).

The shape of the simulated  $H\beta$  PNLF would be more adequate for shape tests (see Fig. 6); unfortunately the nebular recombination lines ( $H\alpha$  would be the natural choice) are more difficult to measure than  $\lambda 5007$ .

## 8. On maximum final masses

Fig. 9 shows our PNLF simulations for different maximum final masses. The reason for the different shapes is easy to understand: the more massive central stars tend to accumulate at the brightest (resp. faintest) magnitudes when they are on heating (resp. cooling) tracks. Therefore, when we eliminate them, the relative percentage of central stars at intermediate magnitudes (from  $-4$  to  $0$ ) increases. This dependence of the PNLF shape on the maximum final mass is what may allow us to learn about maximum final masses in many different galaxies when suitably equipped 8-m telescopes become available. It will be a slow trial-and-error process, because at the same time we will have to test whether or not the simulated PNLFs produce acceptable and consistent fits. For example, one critical assumption needed to derive maximum final masses is that we can use the same value of  $\mu_{\max}$  for all galaxies. For the mo-

ment, the fact that in the present work we find the same  $\mu_{\max}$  for the LMC and M 31 encourages us to expect this parameter to be valid everywhere. But we still have to verify if  $\mu_{\max} = 1$  is statistically consistent with the morphology of excitation diagrams (plots of  $I(5007)$  as function of  $M_{\beta}$ ) made from observations in several different galaxies.

Notice that the effect of the maximum final mass is quite different from the sample size effect: Fig. 10 shows, for comparison, simulated PNLFs that correspond to several sample sizes. Besides, since a change in distance produces a *horizontal* displacement of the PNLF, there is no problem for a simultaneous determination of distance, sample size and maximum final mass, provided only that the sample size is large enough to produce small statistical fluctuations at the bright end of the PNLF.

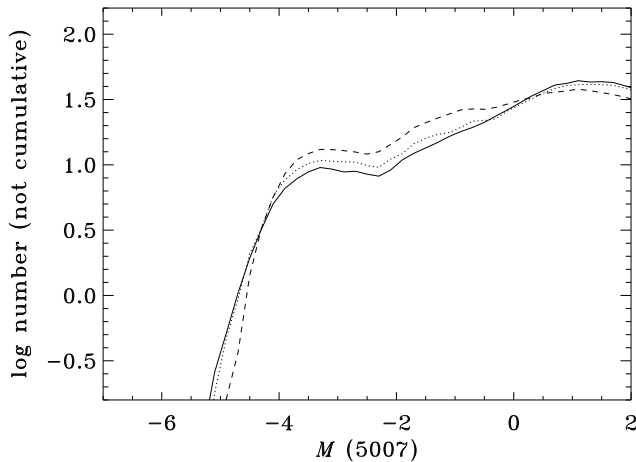


**Fig. 9.** Simulated PNLFs for  $\mu_{\max} = 1$ , sample size = 1000, and three maximum final masses: 1.19 (full line), 0.70 (dotted) and 0.63 solar masses (dashed). In each case the exponential mass distribution has been truncated at the limiting mass.

Using our improved PNLF simulations, we have tried to estimate the maximum final masses in the LMC and the bulge of M 31. Our preliminary estimates are 0.70 and 0.63 solar masses in the LMC and M 31, respectively; see Figs. 11 and 12. This would be consistent with the existence of more recent star formation in the LMC. However, this result is only tentative, due to the small number of available bright PNs, and a confirmation would be desirable. An improvement of the statistics in the case of the LMC is rather unlikely, because we cannot expect to find many more of the bright PNs; we think it is more promising to attempt the collection of PN samples in more luminous galaxies with recent star formation, and to combine those samples in order to further increase the sample size.

Although there is quite a lot of information published or in press about PNLFs in galaxies with recent star formation (see e.g. Jacoby 1997, Feldmeier et al. 1997), it is not suitable for the kind of test we would like to make. Four conditions have to be fulfilled: (1) there must be abundant evidence of recent star formation. This does not necessarily imply a restriction to spiral and irregular galaxies: consider e.g. the blue bulge of

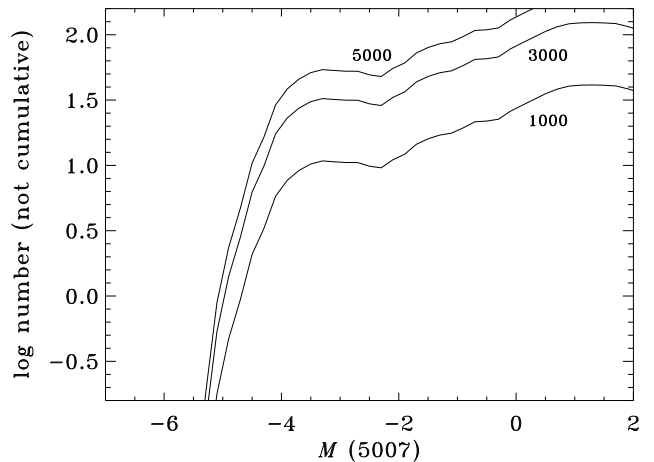


**Fig. 10.** Simulated PNLFs for  $\mu_{\max} = 1$ , maximum final mass = 0.70 solar masses, and three sample sizes: 1000, 3000, 5000.

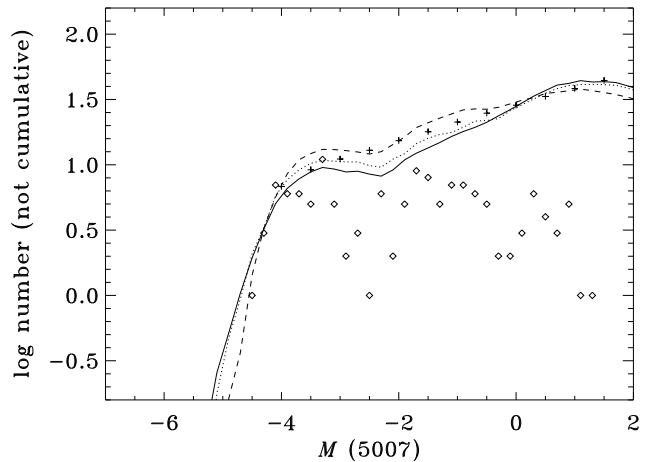


**Fig. 11.** The observed PNLF in the LMC compared with simulations for different maximum final masses. We have overplotted on Fig. 9 the same LMC PNLF used before. The fit is difficult, but it would seem that the best agreement is obtained for a maximum final mass of 0.70 solar masses (dotted). Notice that the curve for 0.63 solar masses (dashed) produces too many PNs at  $-3.7$ .

the lenticular galaxy NGC 5102 (McMillan et al. 1994); (2) the PN searches must have been made without avoiding the regions of recent star formation (for example, we cannot use PNs found in the halos of edge-on spiral galaxies like NGC 891 (Ciardullo et al. 1991) and NGC 4565 (Jacoby et al. 1996), or in the bulges of M 31 and M 81); (3) a statistically complete sample must have been established, extending at least 1.5 mag fainter than the bright end of the PNLF, in order to reach the section of the PNLF where the shape effects are predicted to be most easily detectable; (4) to use PNLF distances for this kind of study would be equivalent to running in circles. A cepheid distance (or any other universally accepted method of distance determination) must be available, in order to eliminate any

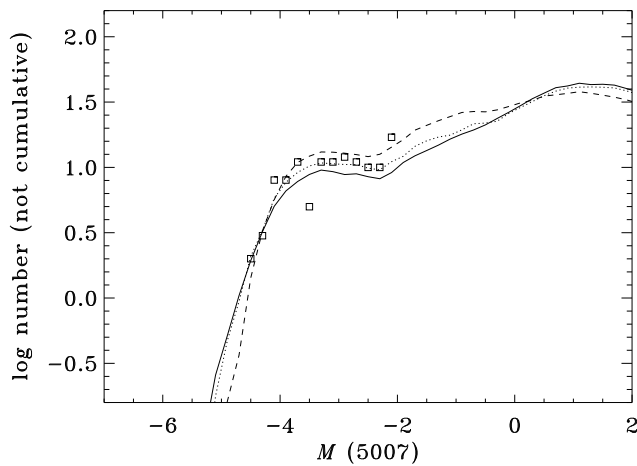


**Fig. 12.** The observed PNLF in M 31 compared with simulations for different maximum final masses. We have overplotted on Fig. 9 the same M 31 PNLF used in Fig. 7. The best agreement is obtained for a maximum final mass of 0.63 solar masses (dashed).

effects derived from the assumption that the PNLF is universal, which is used in the application of the maximum likelihood method for PNLF distance determinations.

It turns out that, of the more than 30 galaxies where many PNs have been found (Jacoby 1997 gives the most up-to-date summary) none satisfies simultaneously the 4 conditions. Of course this does not affect in any significant way the conclusion that cepheid distances and PNLF distances are in excellent agreement; we simply remark that the available samples do not allow us to properly study population effects. So far, the galaxy that comes closer to fulfill the 4 conditions is NGC 300 (Soffner et al. 1996), but the sample size must be substantially increased before NGC 300 can provide a convincing test.

## 9. Conclusion

One positive aspect of these PNLF simulations is that they make some testable predictions, like the possible change of slope at  $M(5007) = -2.3$ , or the relation between the  $\lambda 5007$  and  $H\beta$  (or  $H\alpha$ ) PNLFs, or the morphology of the plots of  $I(5007)$  as function of  $M\beta$  or  $M\alpha$ . Several 8m-class telescopes will soon become available, probably producing explosive progress in the field of extragalactic PNs. Since there will be inevitable efforts to detect many of these objects and obtain their spectra, given their usefulness for distance, kinematic and abundance studies, we can be assured that the predictions will be testable in the near future, leading perhaps to further improvements of the simulated PNLFs. Given deeper PN searches and larger sample sizes, we will then have better chances to decide if there are indeed detectable population effects in the shape of the PNLF, or, if there are not, to understand what are the astrophysical reasons for their absence. In any case, through such work the PNLF may become a more reliable tool for even more accurate extragalactic distance determinations.

## 10. Acknowledgements

This work has been supported by the Deutsche Forschungsgemeinschaft through Grant SFB (Sonderforschungsbereich) 375. We are grateful to J.J. Feldmeier, R. Ciardullo and G.H. Jacoby for showing us data before publication.

## References

- Acker A., Ochsenbein F., Stenholm B. et al. 1992, The Strasbourg-ESO Catalogue of Galactic PN  
 Blöcker T. 1995, A&A 299, 755  
 Blöcker T., Schönberner D. 1990, A&A 240, L11  
 Bragaglia A., Renzini A., Bergeron P. 1995, ApJ 443, 735  
 Ciardullo R. 1995, in Highlights of Astron., Vol. 10, p. 507  
 Ciardullo R., Jacoby G.H., Ford H.C., Neill J.D. 1989, ApJ 339, 53  
 Ciardullo R., Jacoby G.H., Harris W.E. 1991, ApJ 383, 487  
 Dopita M.A., Jacoby G.H., Vassiliadis E. 1992, ApJ 389, 27  
 Feldmeier J.J., Ciardullo R., Jacoby G.H. 1997, ApJ, submitted  
 Jacoby G.H. 1980, ApJS 42, 1  
 Jacoby G.H. 1997, Invited Review in IAU Symp. 180, Planetary Nebulae, in press  
 Jacoby G.H., Ciardullo R., Harris W.E. 1996, ApJ 462, 1  
 Jacoby G.H., Walker A.R., Ciardullo R. 1990, ApJ 365, 471  
 McMillan R., Ciardullo R., Jacoby G.H. 1994, AJ 108, 1610  
 Meatheringham S.J., Dopita M.A. 1991a, ApJS 75, 407  
 Meatheringham S.J., Dopita M.A. 1991b, ApJS 76, 1085  
 Meatheringham S.J., Dopita M.A., Morgan D.H. 1988, ApJ 329, 166  
 Méndez R.H. 1991, in: Michaud G. and Tutukov A. (eds) Proc. IAU Symp. 145, Evolution of Stars: the Photospheric Abundance Connection, Kluwer, p. 375  
 Méndez R.H., Kudritzki R.P., Herrero A. 1992, A&A 260, 329  
 Méndez R.H., Kudritzki R.P., Ciardullo R., Jacoby G.H. 1993, A&A 275, 534 (MKCJ93)  
 Paczynski B. 1971, Acta Astron. 21, 417  
 Schönberner D. 1989, in: Torres-Peimbert S. (ed) Proc. IAU Symp. 131, Planetary Nebulae, Kluwer, p. 463  
 Soffner T., Méndez R.H., Jacoby G.H. et al. 1996, A&A 306, 9  
 Stasinska G. 1989, A&A 213, 274  
 Tylenda R., Stasinska G., Acker A., Stenholm B. 1994, A&AS 106, 559  
 Vassiliadis E., Dopita M.A., Morgan D.H., Bell J.F. 1992, ApJS 83, 87  
 Vassiliadis E., Wood P.R. 1994, ApJS 92, 125  
 Wood P.R., Meatheringham S.J., Dopita M.A., Morgan D.H. 1987, ApJ 320, 178